

**Supplementary Information for:**

**Colloidal Nano-MOFs Nucleate and Stabilize Ultra-Small Quantum Dots of Lead Bromide Perovskites**

Loredana Protesescu,<sup>a,‡</sup> Joaquin Calbo,<sup>b,§</sup> Kristopher Williams,<sup>c</sup> William Tisdale,<sup>c</sup> Aron Walsh,<sup>b,d</sup>  
and Mircea Dincă<sup>a\*</sup>

<sup>a</sup>Department of Chemistry, Massachusetts Institute of Technology, 77 Massachusetts Avenue,  
Cambridge, Massachusetts 02139, United States

<sup>b</sup>Department of Materials, Imperial College London, London SW7 2AZ, United Kingdom

<sup>c</sup>Department of Chemical Engineering, Massachusetts Institute of Technology, 77 Massachusetts  
Avenue, Cambridge, Massachusetts 02139, United States

<sup>d</sup>Department of Materials Science and Engineering, Yonsei University, Seoul 03722, Korea

**Corresponding Author**

\*[mdinca@mit.edu](mailto:mdinca@mit.edu)

**Present Addresses**

<sup>‡</sup>Zernike Institute for Advanced Materials, University of Groningen, Nijenborgh 4, 9747  
AG Groningen Netherlands

<sup>§</sup>Instituto de Ciencia Molecular, Universidad de Valencia, 46890 Paterna, Spain

Table of contents:

1. Materials.....	3
2. Experimental methods.....	3
3. Computational methods.....	5
4. Characterization methods.....	6
Table S1. Synthesis of nano Cr-MIL-101 using various modulators and the morphology of the NPs.....	8
Table S2. The frontier VB and CB energy levels predicted in the DOS of CsPbBr <sub>3</sub> , Cr-MIL-101 and CsPbBr <sub>3</sub> @Cr-MIL-101.....	10
Figure S1. Synthesis of CsPbBr <sub>3</sub> @bulk Cr-MIL-101.....	11
Figure S2. Synthesis of nano Cr-MIL-101.....	12
Figure S3. FTIR spectra for bulk Cr-MIL-101 and colloidal Cr-MI-101.....	13
Figure S4. The importance of the film quality.....	14
Figure S5. Optimization of the Cs:Pb ratio for CsPbBr <sub>3</sub> @nano Cr-MIL-101.....	15
Figure S6. Photoluminescence spectra of CsPbBr <sub>3</sub> @nano Cr-MIL-101, FAPbBr <sub>3</sub> @nano Cr-MIL-101 and MAPbBr <sub>3</sub> @nano Cr-MIL-101.....	16
Figure S7. XRD Comparison between XRD patterns of bulk Cr-MIL-101 (black), nano Cr-MIL-101 (green) and CsPbBr <sub>3</sub> @nano Cr-MIL-101 (blue).....	17
Figure S8. TEM histogram for the size of CsPbBr <sub>3</sub> NCs from 3 similar samples.....	18
Figure S9. Comparison between Raman vibrational bands of bulk Cr-MIL-101, bulk CsPbBr <sub>3</sub> and CsPbBr <sub>3</sub> @nano Cr-MIL-101.....	19
Figure S10. Comparison between Raman vibrational bands of bulk CsPbBr <sub>3</sub> (orange) CsPbBr <sub>3</sub> @nano Cr- MIL-101 (blue) and CsPbBr <sub>3</sub> colloidal NCs 10 nm.....	20
Figure S11. N <sub>2</sub> Absorption isotherm for nano Cr-MIL-101 (black) compared with CsPbBr <sub>3</sub> @nano Cr-MIL-101 (green).....	21
Figure S12. APbX <sub>3</sub> @nano Cr-MIL-101 photoluminescence decay traces .....	22
Figure S13. Photoluminescence spectra for several temperature during the cooling process from 300°K to 80°K.....	23
Figure S14. Molecular orbitals for (a) Cr-MIL-101 and (b) CsPbBr <sub>3</sub> moieties.....	24
Figure S15. The frontier energy levels in CsPbBr <sub>3</sub> @Cr-MIL-101 .....	25
References.....	25

## 1. Materials.

Chromium(III) nitrate nonahydrate (98.5%, Alfa Aesar), terephthalic acid ( $\geq 98\%$ , Alfa Aesar), hydrofluoric acid (48~51 w/v %, BDH Aristar), ammonium fluoride ( $\geq 98\%$ , Sigma-Aldrich), ethanol (99.5%, VWR), N,N'-dimethylformamide (99.5%, Sigma-Aldrich), Methanol (99.9%, VWR), tetrahydrofuran (ACS grade, BDH), and 1,2-dimethoxyethane (99.5%, Sigma-Aldrich), acetic acid (99.7%, Sigma-Aldrich), hexanoic acid ( $>99\%$ , Sigma-Aldrich), benzoic acid ( $>99.5\%$ , Sigma-Aldrich), oleic acid ( $>99\%$ , Sigma-Aldrich), octadecylamine (97%, Sigma-Aldrich), oleylamine ( $>70\%$ , Sigma-Aldrich), CsBr (99.9%, Sigma-Aldrich), FAbBr ( $>99\%$ , Sigma-Aldrich), MABr ( $>99\%$ , Sigma-Aldrich), PbBr<sub>2</sub> (99.999%, Sigma-Aldrich), N-methyl-formamide (99%, Sigma-Aldrich), acetone ( $>99.9\%$ , Sigma-Aldrich) were used as received.

## 2. Experimental methods.

*Synthesis of bulk Cr-MIL-101:* Cr-MIL-101 was prepared according to the procedures reported by Férey et al.<sup>1-2</sup> A typical synthesis involved a mixture of Cr(NO<sub>3</sub>)<sub>3</sub>•9H<sub>2</sub>O (800 mg, 2.00 mmol) and terephthalic acid (332 mg, 2.00 mmol) in 10 ml of water with 0.072 mL (2.0 mmol) of HF. The mixture was introduced to a Parr pressure vessel, which was placed in a convection oven held at 220 °C for 8 h. After natural cooling, the mixture was first passed through a large-pore fritted glass filter to remove the residual terephthalic acid. The filtrate was then passed through a fine-pore filter paper to collect the Cr-MIL-101 product. The obtained Cr-MIL-101 was further purified by two solvent treatments using ethanol and aqueous NH<sub>4</sub>F. The first solvent treatment involved introducing the solid sample to refluxing ethanol until no detection of colored impurities in the mother liquor. The sample was then subjected to an aqueous solution of 30 mM NH<sub>4</sub>F at 60 °C for 10 h. After natural cooling, Cr-MIL-101 was filtered and washed several times with hot water at 60 °C to remove residual NH<sub>4</sub>F.

*Synthesis of nano Cr-MIL-101* was performed using a modified procedure described by Edler group:<sup>3</sup>

- i) Carboxylic acids as modulators: Cr(NO<sub>3</sub>)<sub>3</sub>•9H<sub>2</sub>O (264 mg, 0.66 mmol) and terephthalic acid (108 mg, 0.66 mmol) and 15 ml of water were placed in a Parr pressure vessel and reacted for 15 h at 180 °C. One of the modulators (acetic acid, hexanoic acid, benzoic acid and oleic acid) was added to the rest of the precursors using 3 quantities to established the best protocol (0.055 mmol, 0.11 mmol and 0.22 mmol). The best results were obtained with oleic acid (0.055 mmol). After natural cooling, the mixture was first passed through a large-pore fritted glass filter to remove the residual terephthalic acid. The green powder was then saved in 45 mL centrifuge tubes for washing. Washing procedure was carried out using 10 mL acetone to redisperse the MOF NPs and hexane or toluene for reprecipitation (2 mL or until cloudy suspension). This procedure was repeated once again.

- ii) Primary amines as modulators:  $\text{Cr}(\text{NO}_3)_3 \cdot 9\text{H}_2\text{O}$  (264 mg, 0.66 mmol), terephthalic acid (108 mg, 0.66 mmol) and 15 ml of water were placed in a Parr pressure vessel and reacted for 15 h at 180 °C. One of the modulators (oleylamine, octadecylamine) was added to the rest of the precursors using 3 quantities to establish the best protocol (0.055 mmol, 0.11 mmol and 0.22 mmol). After natural cooling, the mixture was first passed through a large-pore fritted glass filter to remove the residual terephthalic acid. The green powder was then saved in 45 mL centrifuge tubes for washing. Washing procedure was carried out using 10 mL acetone to redisperse the MOF NPs and hexane or toluene for reprecipitation (2 mL or until cloudy suspension). This procedure was repeated once again.

*Synthesis of  $\text{APbBr}_3@$ nano Cr-MIL-101*: Standard solution of 0.05 M in NMF were prepared in advance for CsBr,  $\text{PbBr}_2$ , FABr and MABr. 50 mg/mL suspension of nano Cr-MIL-101 in MFA was prepared after washing and drying the NPs from acetone. 100  $\mu\text{L}$  suspension of MOF was mixed with a total of 100  $\mu\text{L}$  of mixed solution of A cation and  $\text{PbBr}_2$ . During the screening the Cs:Pb ratio was tested for 1:2, 1:1.5, 1:1, 1.5:1, and 2:1 while for FA and MA the ratio was kept to 1:1. The solution was drop casted on a glass substrate (washed with acetone/ethanol) on a hot plate preheated at 70 °C and dried for 1 min. The final films were further investigated. Additionally, thin films were prepared using a spin coater, at 1000 rpm, with an IR lamp fixed on top of the rotor and fixed the temperature at 100 °C. Up to 5 layers were applied to vary the thickness.

Example of  $\text{CsPbBr}_3@$ nano Cr-MIL-101 synthesis: 100  $\mu\text{L}$  nano Cr-MIL-101 (50 mg/mL) was mixed with 50  $\mu\text{L}$  CsBr solution (0.05 M in NMF) and 25  $\mu\text{L}$   $\text{PbBr}_2$  solution (0.05 M in NMF). The solution was stirred for 12 h at room temperature. For the 1 cm x 1 cm glass substrate, 50  $\mu\text{L}$  of the prepared solution was spin-coated at 1000 rpm using the top applied heating. The film was further heated on a hot plate for 1 min at 70 °C. The film deposition procedure was repeated 3 times to increase the thickness.

The colloidal  $\text{CsPbBr}_3$  NCs for Raman study were synthesized via hot injection method according to literature.<sup>4</sup>

### 3. Computational methods.

Among the two pores of Cr-MIL-101, the smaller M pore cage was selected in our calculations. Terminal ligands were cut and modelled as formate groups ( $\text{HCOO}^-$ ), whereas one F atom and two water molecules were inserted per inorganic cluster for completing Cr coordination and achieving charge neutrality. In total, cluster M cage modelled contains 1530 atoms. Spin moment for each Cr atom was set to 3 (high-spin configuration) in all calculations. The lead halide perovskite (LHP) nanoparticle of  $\text{CsPbBr}_3$  was initially modelled in the cubic phase and with the size that allows encapsulation into the M cage of Cr-MIL-101. The  $\text{CsPbBr}_3$  NP modelled contains 136 atoms with

dimensions of ca. 1.5 x 1.5 x 1.5 nm and its total charge is zero ( $\text{Cs}_{27}\text{Pb}_{27}\text{Br}_{81}$ ). Minimum-energy geometries for the cluster models of Cr-MIL-101 and  $\text{CsPbBr}_3$  were obtained at the PBESol<sup>5</sup> level of theory with the “tier 1” basis set by means of the FHI-AIMS suite of programs.<sup>6</sup> Relativistic effects were considered through the atomic ZORA approximation.<sup>6</sup> Electronic structure single-point calculations were then performed using the HSE06<sup>7</sup> hybrid functional with “tier 1” basis set. The electronic density of states (DOS) as well as the corresponding atom projection was obtained at the same level of theory, and a post-SCF spin-orbit coupling was included for the LHP NP system. Molecular orbitals were plotted using VESTA.<sup>8</sup>

We used an embedding-inverted approach to simulate the effect of the perovskite (considered as monopole charges) into the energy levels of Cr-MIL-101. Fixed atomic charges for each LHP NP atom were set in each atomic position with a value according to the Mulliken charge analysis for the isolated nanoparticle. Before geometry relaxation, we predict a slight narrowing of the bandgap, but the frontier energy levels remain practically unchanged after relaxation (Table S2). As expected, the electronic structure of Cr-MIL-101, including the bandgap, is barely affected by the encapsulated perovskite NP.

Finally, the binding energy for the perovskite-MOF interaction was computed. The LHP NP was initially placed in the centre of the Cr-MIL-101 M-cage. The geometry optimization calculation of the whole system ( $\text{CsPbBr}_3$ @Cr-MIL-101 with all explicit atoms) was undertaken at the PBESol level of theory with the “tier 1” basis set. The Broyden-Fletcher-Goldfarb-Shanno (BFGS) optimization algorithm was used with a maximum residual force component per atom of 0.01 eV/Å. Geometry optimization proceeds through two steps: i) perovskite and MOF accommodation to avoid steric hindrance between them, and ii) short contacts formation. After full geometry optimization, the binding energy was obtained as the energy difference between the composite and the constituting moieties (Cr-MIL-101 and  $\text{CsPbBr}_3$ ) at their minimum-energy geometries. The latest Grimme’s dispersion correction D3 with the Becke-Johnson damping function<sup>9-10</sup> was applied to account for the long-range noncovalent interactions that stabilize the composite, which amounts –1.2 eV. In total, the binding energy for the perovskite NP-MOF interaction is calculated to be –2.4 eV.

#### 4. Characterization methods

*UV-vis-NIR spectroscopy:* Spectra were collected between 400 and 2275 nm on a Cary 5000i spectrophotometer at a scan rate of 400 nm/min using a PIKE Technologies DiffusIR accessory. For the powder samples which were ground with KBr in a mortar and pestle to a 1 wt% dilution. Spectra were normalized to a 100% KBr baseline, and the Kubelka–Munk equation was applied. The Kubelka–Munk function transformed spectra were then normalized with respect to  $F(R)$  at 400 nm ( $25,000 \text{ cm}^{-1}$ ). For films and solutions, the measurements were taken in transmission mode, using 1 cm cuvettes and cuvettes and film accessory.

*Temperature-dependent and time-resolved photoluminescence* experiments were carried out in a microscope cryostat (Janis, ST-500) under vacuum ( $<1 \times 10^{-4}$  mbar) between 77 and 298 K. Films were photoexcited using a 405 nm laser diode (Picoquant, 5 MHz, 1.01 pJ/pulse, 590 ps pulse duration) which was focused onto the sample surface using an objective lens (Nikon, 40 $\times$ , 0.6 NA) to spot size of 2.8  $\mu\text{m}$ . Epifluorescence from the films was collected through the same objective and sent to a spectrograph (Princeton Instruments, SP-2500, 0.5 m focal length) and spectrally dispersed using a 300 g/mm, 500 nm blaze grating. Static spectra were recorded using a calibrated CCD camera (Princeton Instruments, PIXIS). Time resolved data was recorded using time-correlated single photon counting (TCSPC). The dispersed light from the spectrograph grating was projected through a slit onto an avalanche photodiode (Micro Photon Devices, PDM). This setup allowed for single wavelength detection ( $\pm 1$  nm) of the PL lifetime. Spectrally-resolved lifetime experiments were collected by stepping the grating in 1 nm increments so the lifetime could be recorded at each wavelength from 420 to 560 nm. Otherwise, static room temperature PL measurements were carried out on the same experimental setup using spin-cast films in an ambient environment.

*Powder X-ray diffraction (PXRD) patterns* were recorded on a Bruker Advance II diffractometer equipped with  $\theta/2\theta$  Bragg-Brentano geometry and Ni-filtered Cu-K $\alpha$  radiation ( $K\alpha_1 = 1.5406 \text{ \AA}$ ).

*Surface area measurements* were conducted on a Micromeritics ASAP 2020 Surface Area and Porosity Analyzer. In an Argon glovebox, each activated sample was loaded in an oven-dried sample tube of known mass, which was weighed again to determine the sample mass. The tube was equipped with a S3 TranSeal<sup>TM</sup> (Micromeritics) and transferred out of the glovebox. The sample was placed on the analysis port of the instrument and evacuated at room temperature for 2 hours. N<sub>2</sub> isotherms were measured using liquid nitrogen baths (77 K). UHP grade (99.999% purity) N<sub>2</sub> and He, oil-free valves and gas regulators were used for all free space corrections and measurements. BET surface area was determined using Micromeritics fitting software and MOF specific criteria.

*Raman Spectroscopy*: The Raman measurements were taken using The Horiba LabRam Evolution at the Harvard Center for Nanoscale Systems (Cambridge, MA, USA) with 532 laser excitation, 10% power, 100X magnification.

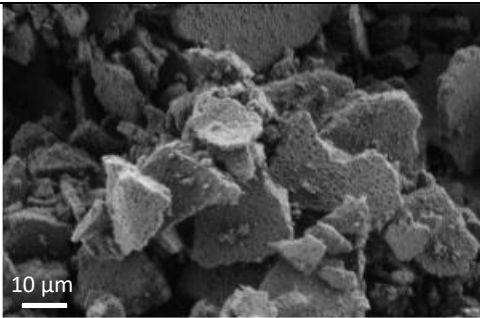
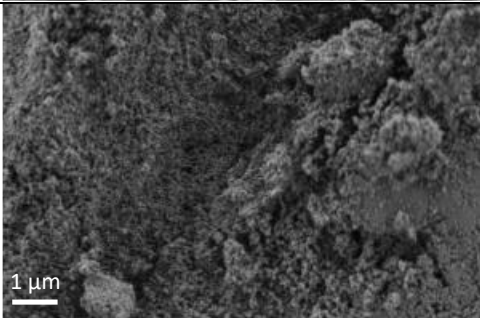
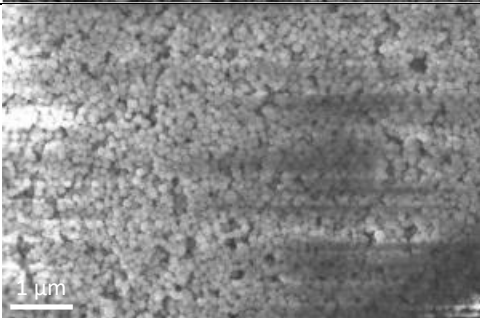
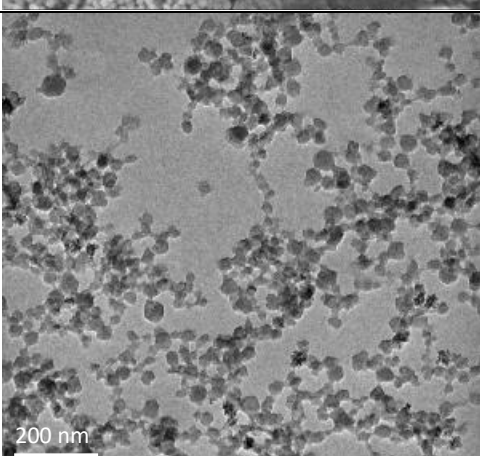
*Attenuated total reflectance infrared (ATR-IR)* absorption spectra were acquired on a Bruker Tensor 37 using ATR accessory. Data were averaged over 16 scans between 3500  $\text{cm}^{-1}$  and 400  $\text{cm}^{-1}$ .

*Transmission electron microscopy (TEM)* was performed on a JEOL 2100 instrument at the Harvard Center for Nanoscale Systems (Cambridge, MA, USA) operating at 200 kV. Samples were prepared on ultrathin Cu support with C type A 400 mesh, using powdered material sonicated in acetone (nano-MOFs) or toluene for LHP@MOFs.

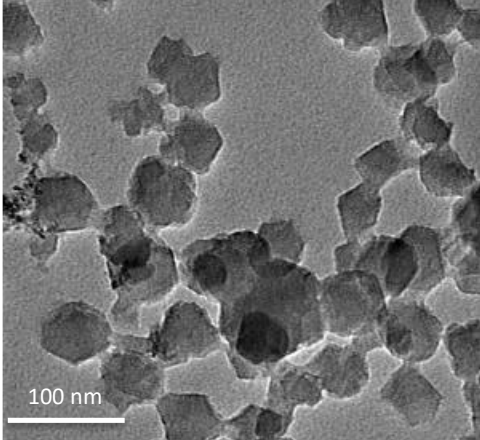
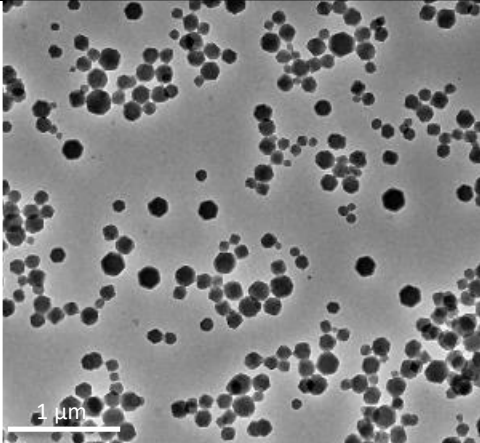
*Scanning electron microscopy (SEM)* was conducted at the Harvard Center for Nanoscale Systems (Cambridge, MA, USA) on a Zeiss Ultra 55 SEM with an InLens detector and an operating voltage of 3 kV.

*Scanning transmission electron microscopy X ray diffraction (STEM EXD) mapping* experiments were performed on JEOL ARM 200F STEM at the Harvard Center for Nanoscale Systems (Cambridge, MA, USA) at 200 kV using similar sample preparation as for TEM experiments.

**Table S1.** Synthesis of nano Cr-MIL-101 using various modulators and the morphology of the NPs

<i>Sample</i>	<i>Modulator</i>	<i>Morphology</i>	<i>SEM/TEM</i>
1	Acetic acid	Porous plates, micron sized	
2	Hexanoic acid	>50 nm NPs, poor colloidal stability in acetone and NMF	
3	Benzoic acid	>80 nm NPs with octahedral shape	
4	Oleic acid	Approx. 25 nm NPs with good size distribution and high colloidal stability in acetone and NMF	



5	Oleylamine	Around 50 nm NPs with poor colloidal stability in acetone and NMF	 <p>100 nm</p>
6	No additive	Polydisperse >80 nm NPs with poor colloidal stability in acetone and NMF	 <p>1 μm</p>

**Table S2.** Frontier energy levels (in eV) of CsPbBr<sub>3</sub>, Cr-MIL-101 and the CsPbBr<sub>3</sub>@Cr-MIL-101 composite (considering the LHP NP as monopoles) at the HSE06 level. Values without (NoSOC) and with (SOC) spin-orbit coupling correction are indicated for CsPbBr<sub>3</sub>.

	CsPbBr <sub>3</sub>		Cr-MIL-101		CsPbBr <sub>3</sub> @Cr-MIL-101	
	$\alpha/\beta$		$\alpha$	$\beta$	$\alpha$	$\beta$
	NoSOC	SOC				
VB	-6.15	<b>-6.06</b>	-5.76	-6.75	-5.74	-6.77
CB	-2.76	<b>-3.25</b>	-3.25	-3.58	-3.23	-3.56
Gap	3.39	<b>2.83</b>	2.51	3.17	2.51	3.21
			2.18		2.18	

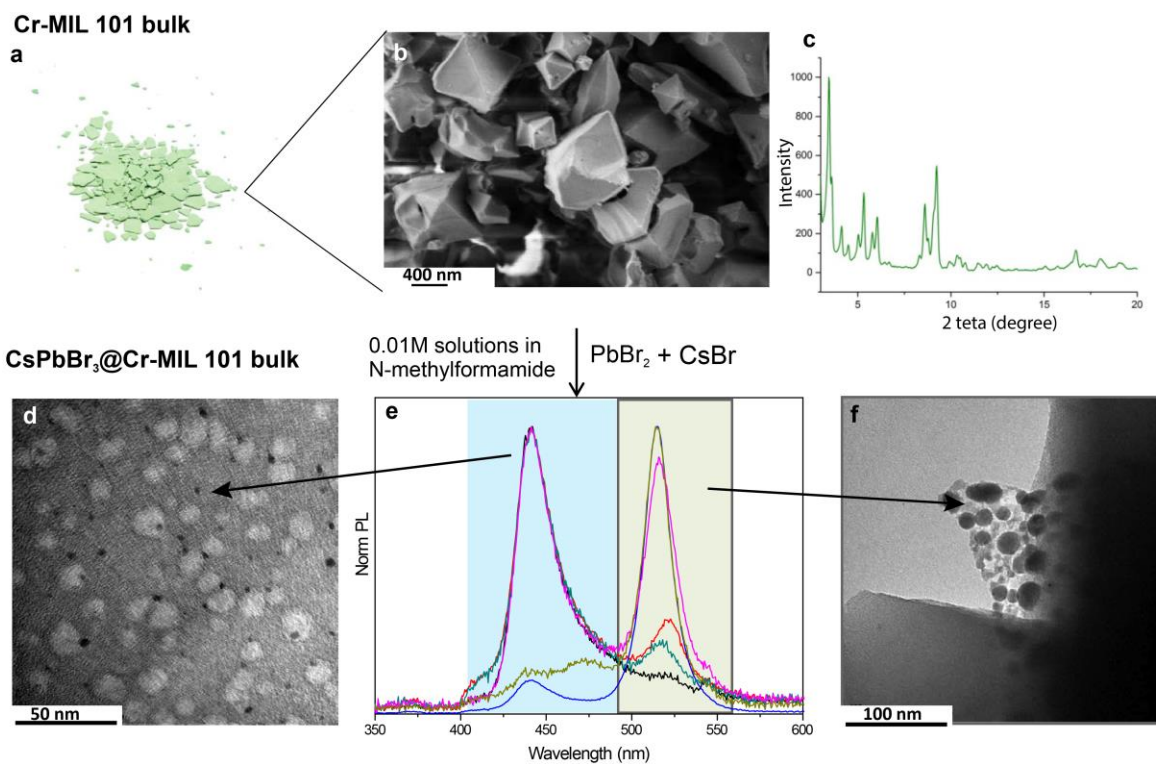


**Figure S1.** Synthesis of CsPbBr<sub>3</sub>@bulk Cr-MIL-101. (a) powder of bulk Cr-MIL-101, (b) SEM images for bulk Cr-MIL-101 showing micron sized octahedrally shaped crystals, (c) XRD pattern for bulk Cr-MIL-101, (d) TEM image showing the small 3 nm CsPbBr<sub>3</sub> form into the pores of Cr-MIL-101, (e) Normalized photoluminescence spectra for CsPbBr<sub>3</sub>@bulk Cr-MIL-101 at various Cs:Pb ratios and LHP:MOF ratio., (f) TEM image showing >20 nm large CsPbBr<sub>3</sub> crystals formed on the surface of the MOF.

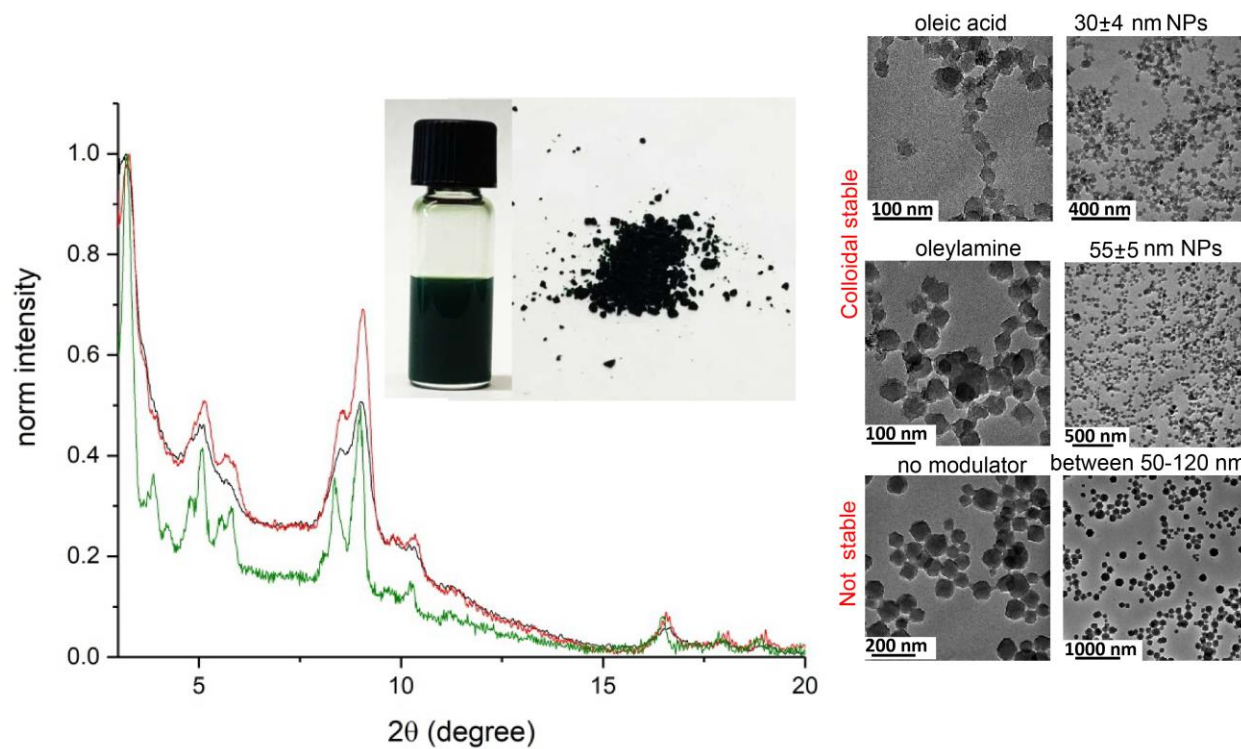


**Figure S2.** Synthesis of nano Cr-MIL-101. XRD patterns nano Cr-MIL-101 when no modulator was used (green pattern), oleic acid was used (red pattern) and oleylamine was used (black pattern) Inset is presented the colloidal solution and dried powder of nano Cr-MIL-101 with oleic acid as modulator. In the right side the TEM images of the corresponding samples are shown.

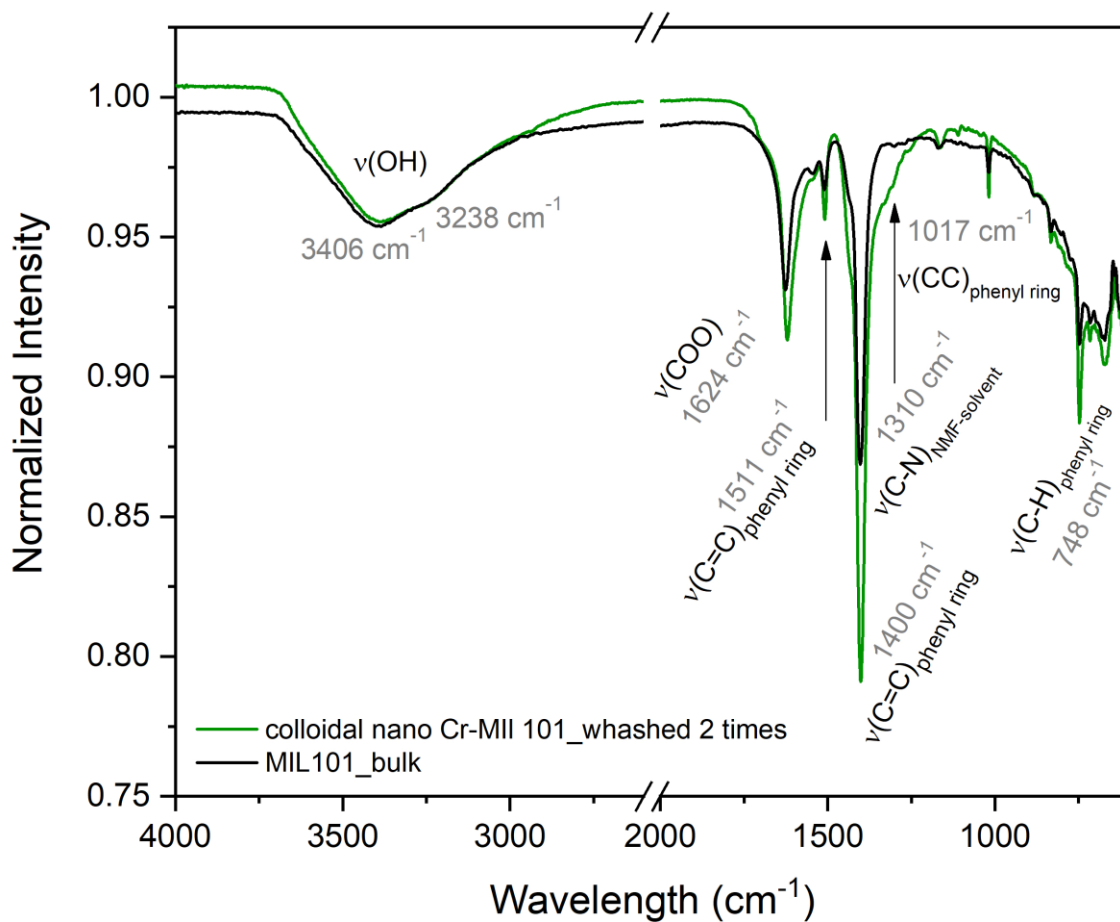


**Figure S3.** FTIR spectra for bulk Cr-MIL-101 (black) and colloidal Cr-MIL-101 (green) after 2 steps of washing with acetone/hexane and redissolve in NMF. All the vibrational bands are assigned and no free  $\text{COO}^-$  corresponding to oleic acid is observed around  $1700 \text{ cm}^{-1}$ .

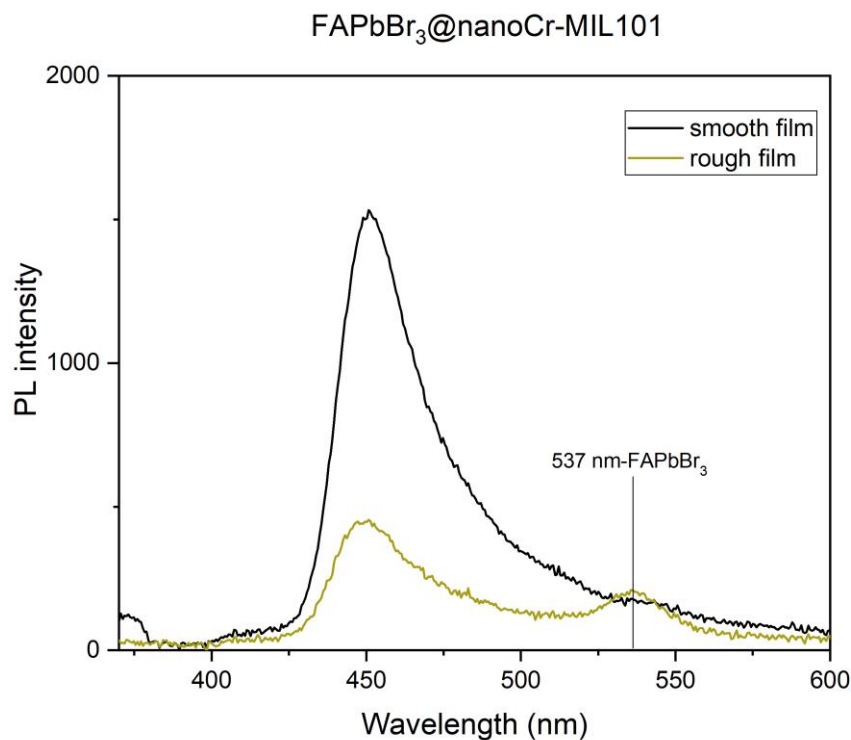


**Figure S4.** The importance of the film quality to minimize the formation of bulk-like emission (537 nm for FAPbBr<sub>3</sub>). At 450 nm is observed the emission of 3 nm FAPbBr<sub>3</sub>@nano Cr-MIL-101. The smooth film was obtained via spincoating at 100 °C of 3 layers of the mother solution (FABr, PbBr<sub>2</sub> 0.05M in NMF, nano Cr-MIL-101 (50 mg/mL) in equal volumes).

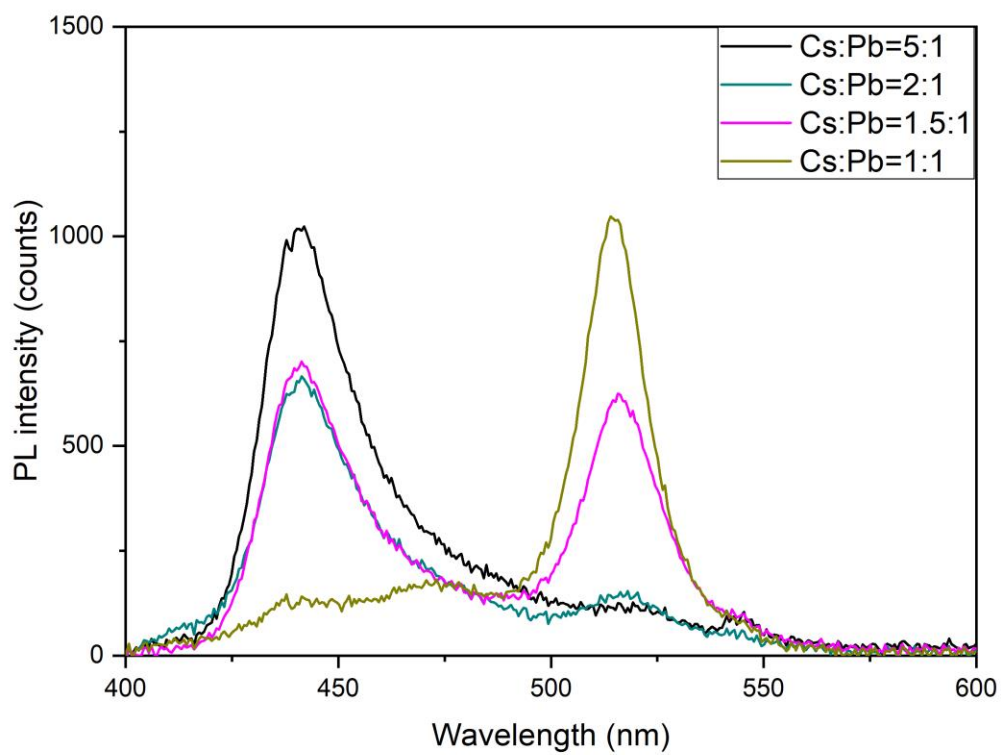


**Figure S5.** Optimization of the Cs:Pb ratio for CsPbBr<sub>3</sub>@nano Cr-MIL-101.

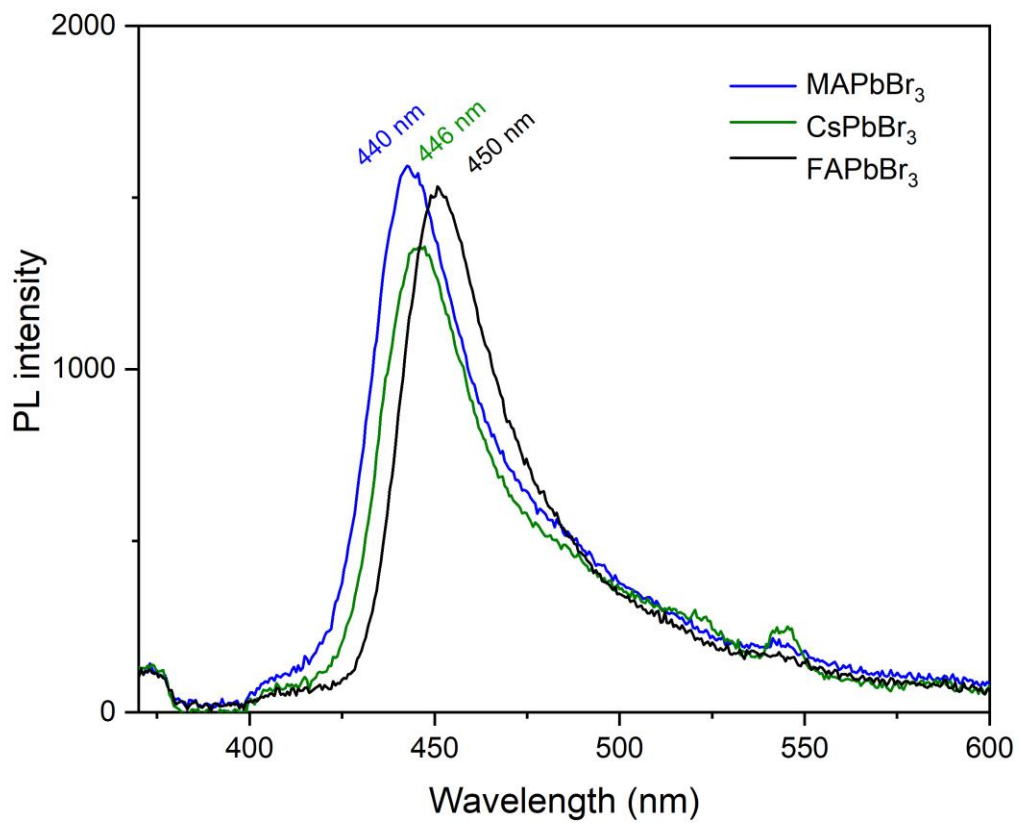


**Figure S6.** Photoluminescence spectra of CsPbBr<sub>3</sub>@nano Cr-MIL-101, FAPbBr<sub>3</sub>@nano Cr-MIL-101 and MAPbBr<sub>3</sub>@nano Cr-MIL-101.



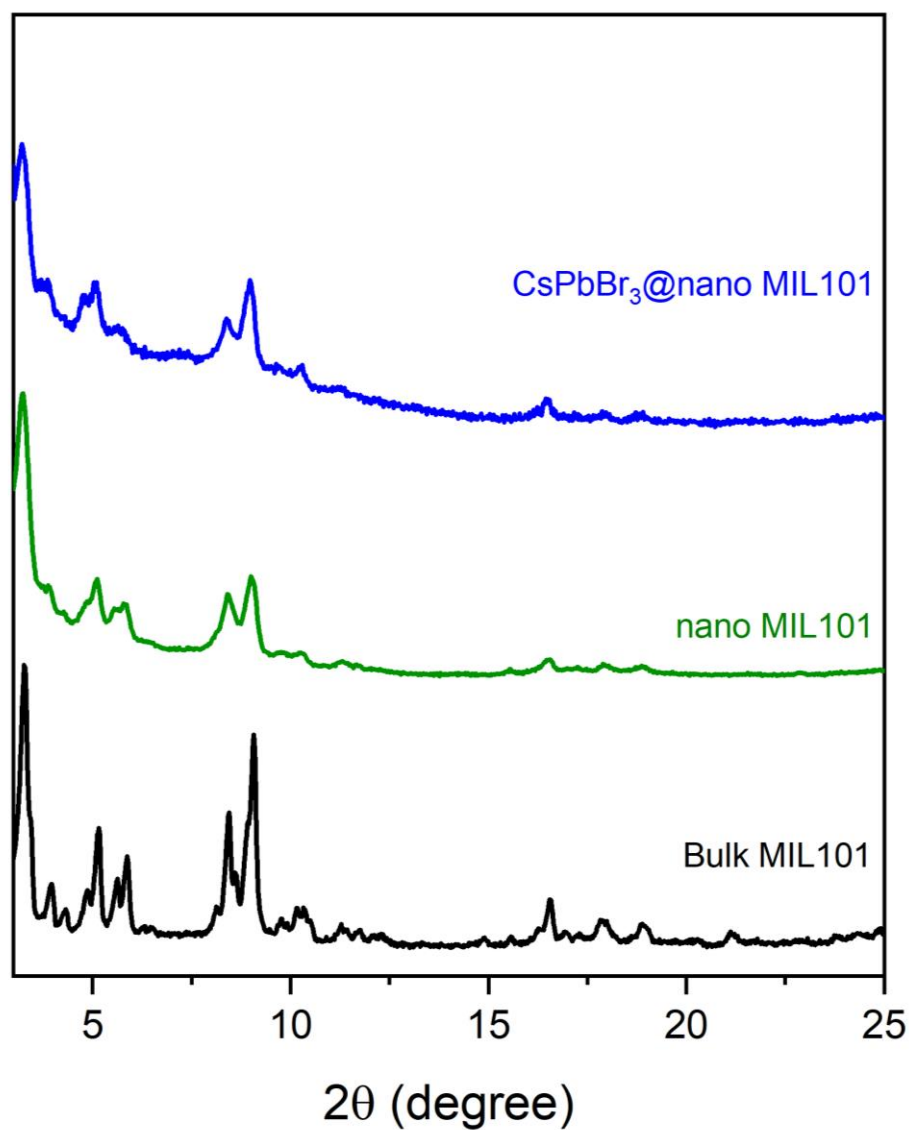


**Figure S7.** XRD Comparison between XRD patterns of bulk Cr-MIL-101 (black), nano Cr-MIL-101 (green) and CsPbBr<sub>3</sub>@nano Cr-MIL-101 (blue). The crystallinity of Cr-MIL-101 nanosized (25 nm) is retained. After the encapsulation of CsPbBr<sub>3</sub>, the MOF structure is not affected. The CsPbBr<sub>3</sub> QDs is not detected by XRD due to extremely small size of the NCs (3 nm).

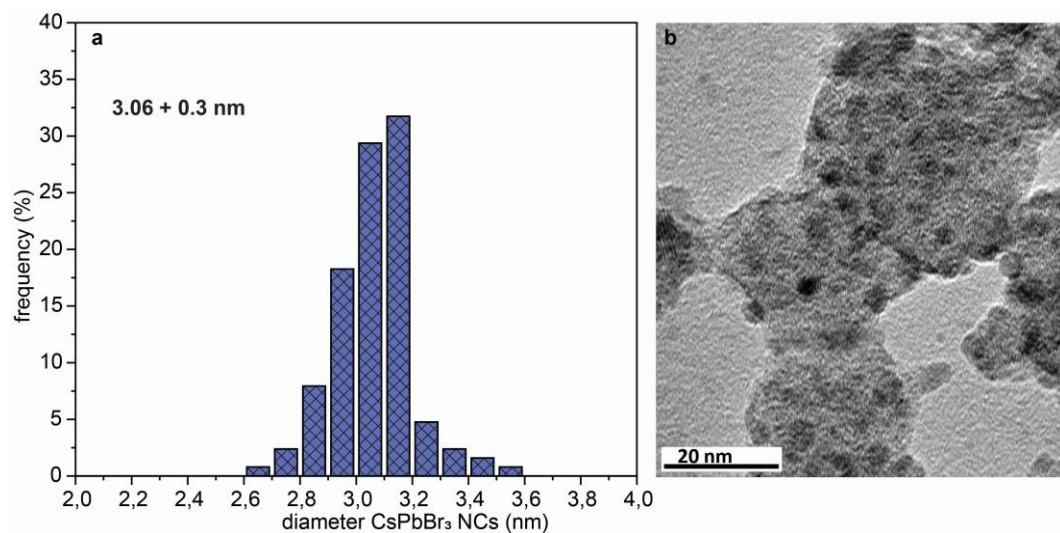


**Figure S8.** a) TEM histogram for the size of CsPbBr<sub>3</sub> NCs in from 3 similar samples. b) Typical TEM image of CsPbBr<sub>3</sub>@nano Cr-MIL-101 used for the histogram counts.

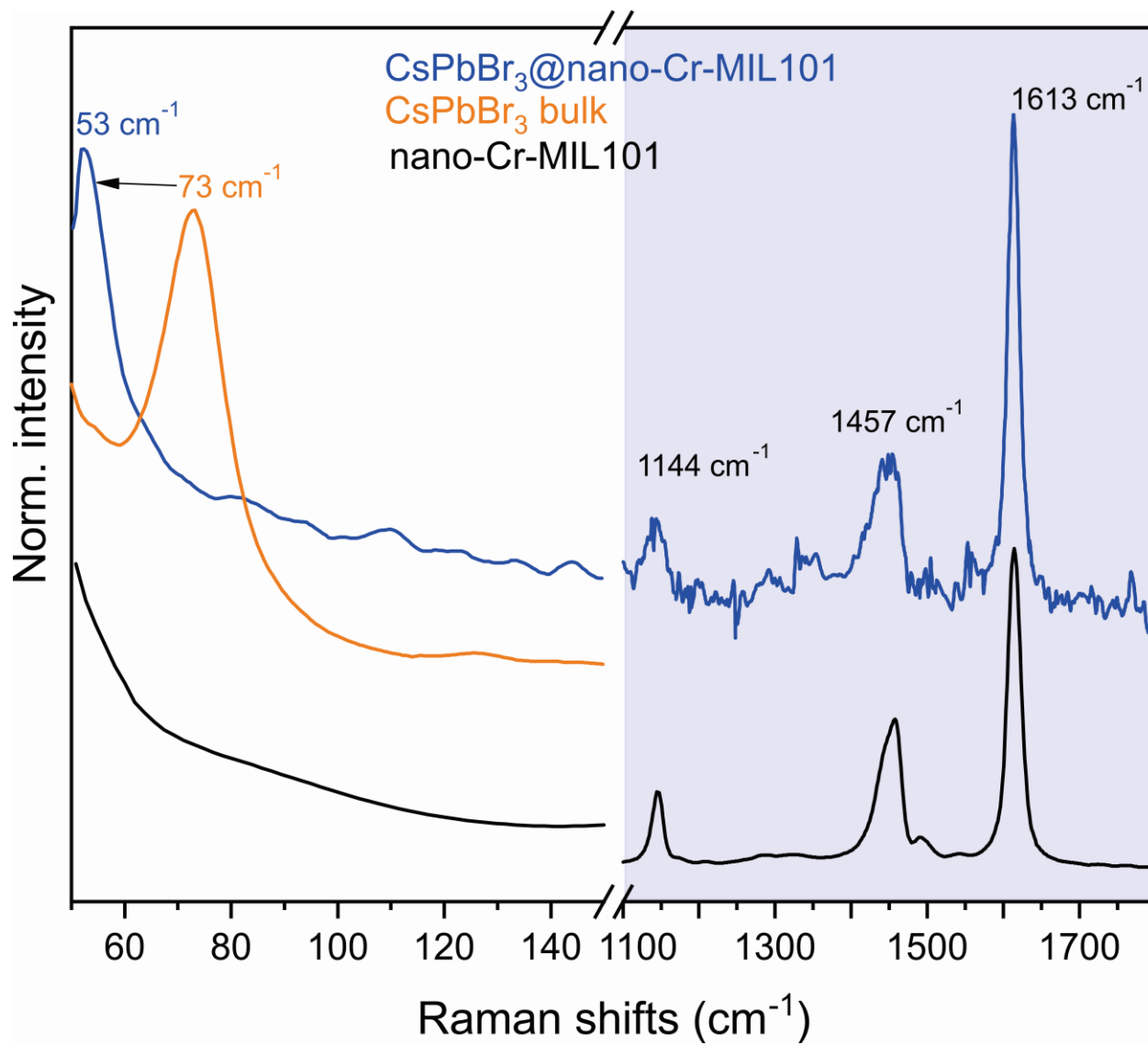


**Figure S9.** Comparison between Raman vibrational bands of bulk Cr-MIL-101 (black), bulk CsPbBr<sub>3</sub> (orange) and CsPbBr<sub>3</sub>@nano Cr-MIL-101 (blue).

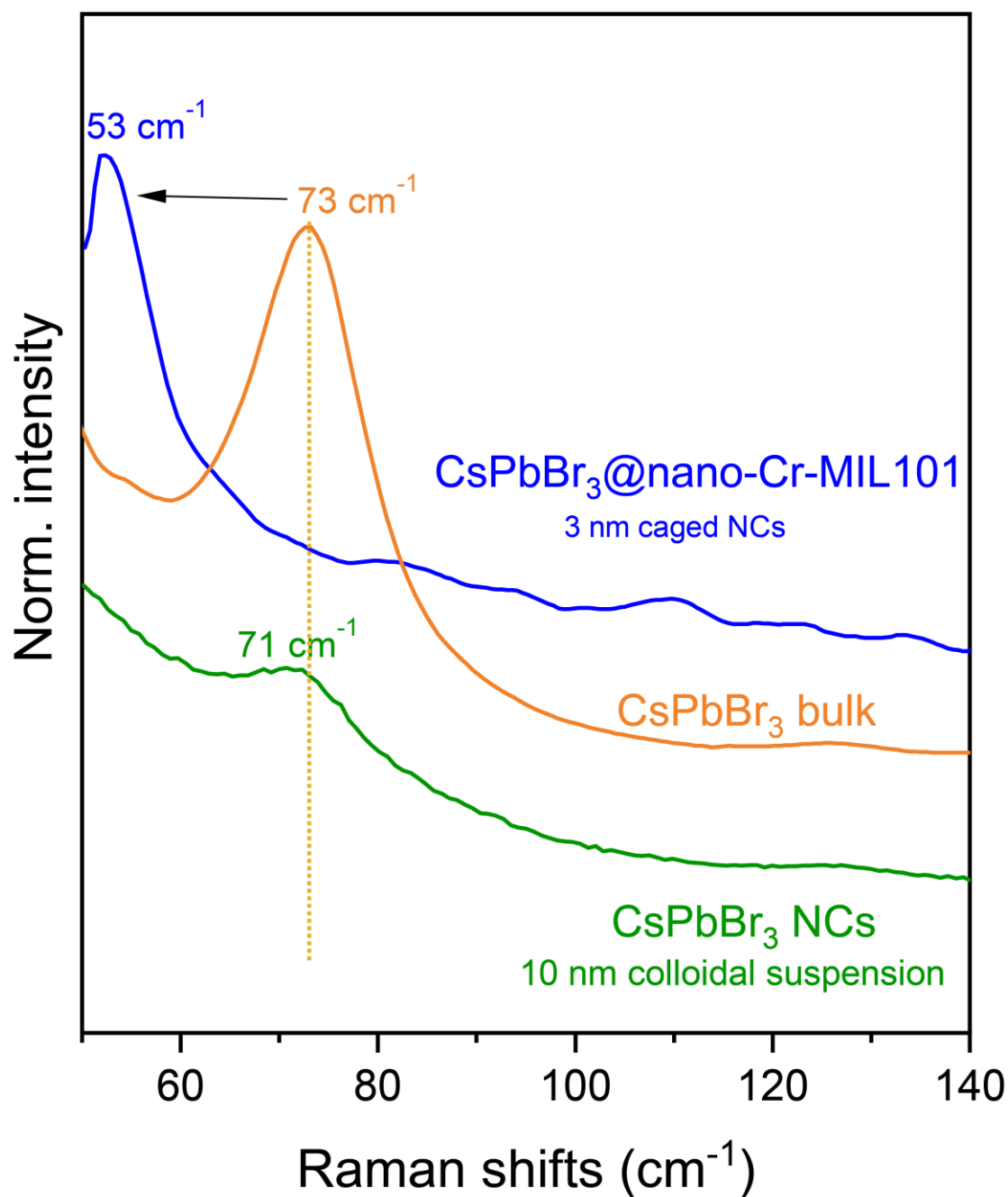


**Figure S10.** Comparison between Raman vibrational bands of bulk  $\text{CsPbBr}_3$  (orange),  $\text{CsPbBr}_3$ @nano Cr-MIL-101 (blue) and  $\text{CsPbBr}_3$  colloidal NCs 10 nm.

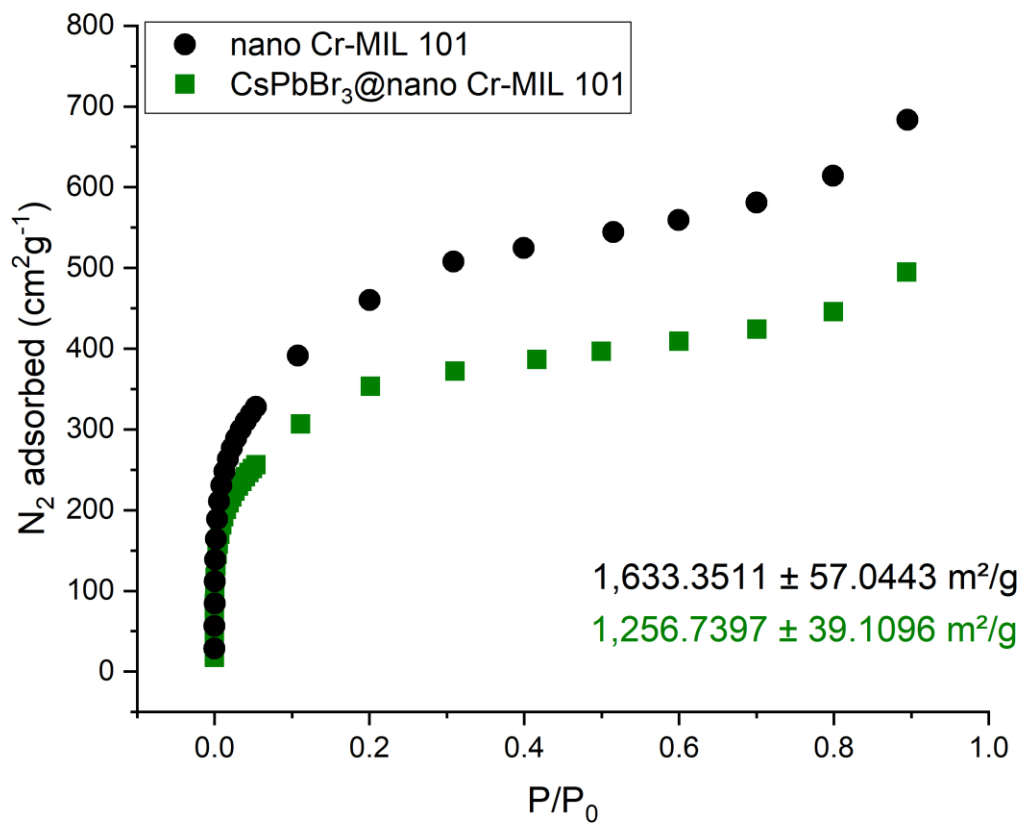


**Figure S11.** N<sub>2</sub> Adsorption isotherm for nano Cr-MIL-101 (black) compared with CsPbBr<sub>3</sub>@nano Cr-MIL-101 (green).

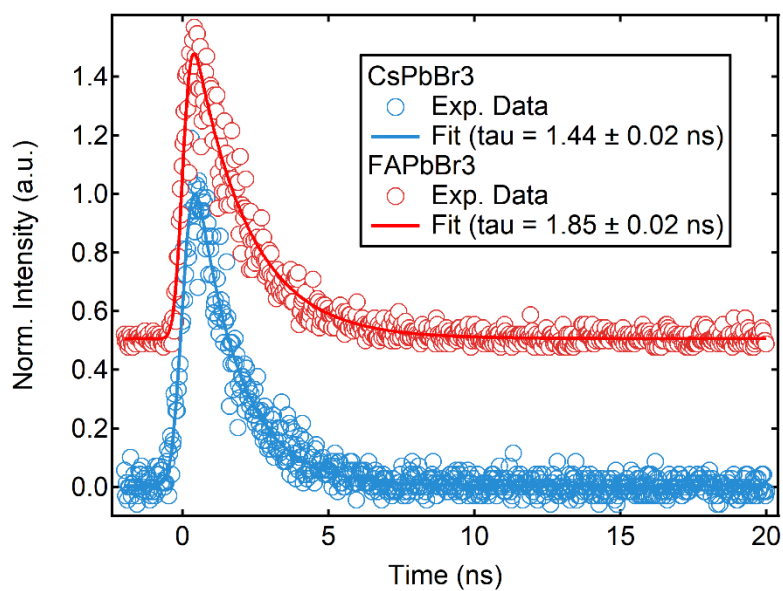


**Figure S12.** APbX<sub>3</sub>@nano Cr-MIL-101 photoluminescence decay traces (open circles) for CsPbBr<sub>3</sub> and FAPbBr<sub>3</sub> taken at the peak emission wavelength (400 nm and 450 nm, respectively) ± 2 nm. Single exponential fits convolved with the laser pulse duration (solid lines) for each experimental trace are also shown.

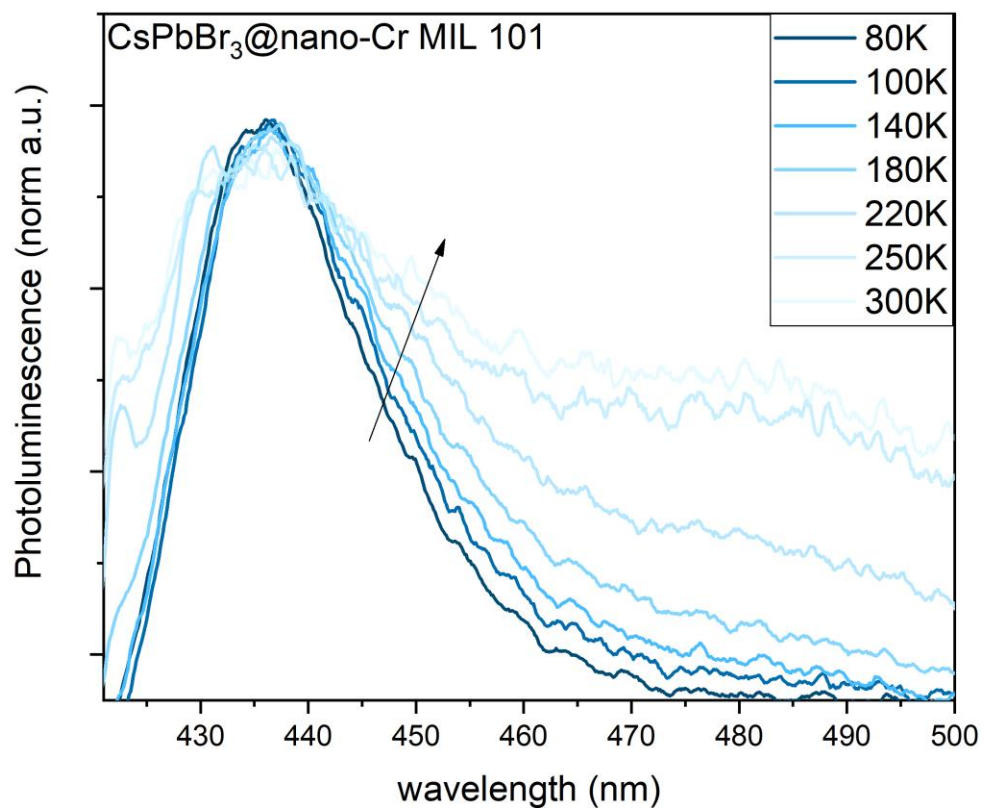
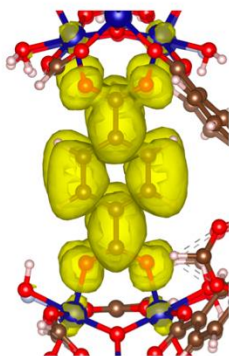


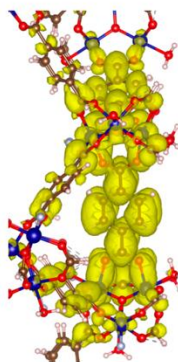
**Figure S13.** Photoluminescence spectra for several temperatures during the cooling process from 300 °K to 80 °K. It shows the broadening of the peaks with increasing the temperature at longer wavelength giving indication of energy transfer from QDs sitting in small pores (2.9 nm) to QDs from the larger pores (3.4 nm).

a. Cr-MIL-101

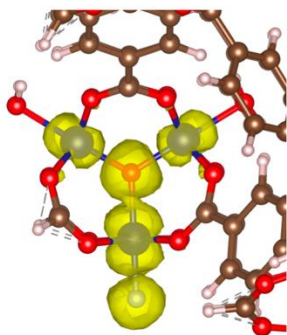
CB (alpha)



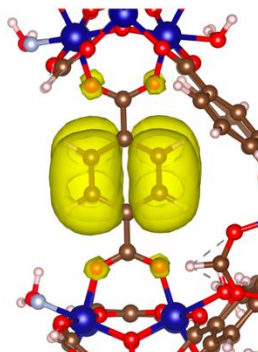
CB (beta)



VB (alpha)

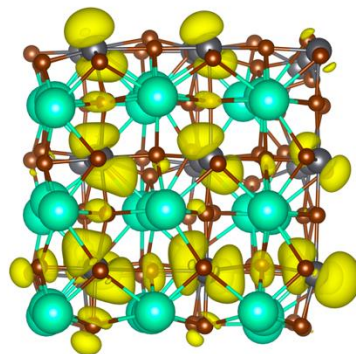


VB (beta)



b. CsPbBr<sub>3</sub>

CB (Pb *p* orbitals)



VB (Br *p* orbitals)

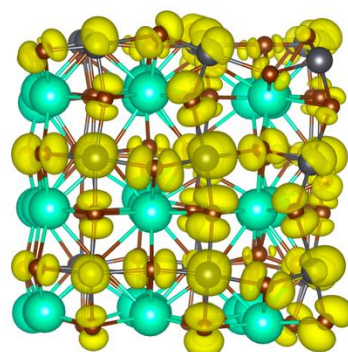


**Figure S14.** Frontier molecular orbitals for (a) Cr-MIL-101 and (b) CsPbBr<sub>3</sub> clusters.



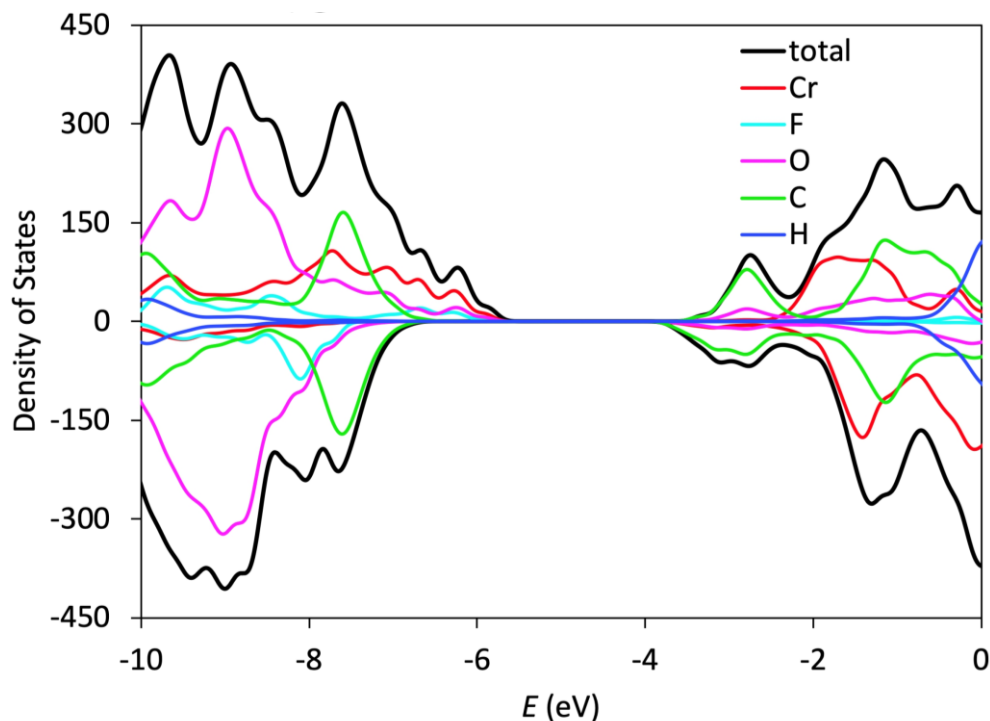


**Figure S15.** The projected density of states of CsPbBr<sub>3</sub>@Cr-MIL-101.

### References:

1. Férey, G.; Mellot-Draznieks, C.; Serre, C.; Millange, F.; Dutour, J.; Surblé, S.; Margiolaki, I., A Chromium Terephthalate-Based Solid with Unusually Large Pore Volumes and Surface Area. *Science* **2005**, *309* (5743), 2040-2042.
2. Hong, D.-Y.; Hwang, Y. K.; Serre, C.; Férey, G.; Chang, J.-S., Porous Chromium Terephthalate MIL-101 with Coordinatively Unsaturated Sites: Surface Functionalization, Encapsulation, Sorption and Catalysis. *Advanced Functional Materials* **2009**, *19* (10), 1537-1552.
3. Jiang, D.; Burrows, A. D.; Edler, K. J., Size-controlled synthesis of MIL-101(Cr) nanoparticles with enhanced selectivity for CO<sub>2</sub> over N<sub>2</sub>. *CrystEngComm* **2011**, *13* (23), 6916-6919.
4. Protesescu, L.; Yakunin, S.; Bodnarchuk, M. I.; Krieg, F.; Caputo, R.; Hendon, C. H.; Yang, R. X.; Walsh, A.; Kovalenko, M. V., Nanocrystals of Cesium Lead Halide Perovskites (CsPbX<sub>3</sub>, X = Cl, Br, and I): Novel Optoelectronic Materials Showing Bright Emission with Wide Color Gamut. *Nano Lett.* **2015**, *15* (6), 3692-6.
5. Perdew, J. P.; Ruzsinszky, A.; Csonka, G. I.; Vydrov, O. A.; Scuseria, G. E.; Constantin, L. A.; Zhou, X.; Burke, K., Restoring the Density-Gradient Expansion for Exchange in Solids and Surfaces. *Physical Review Letters* **2008**, *100* (13), 136406.
6. Blum, V.; Gehrke, R.; Hanke, F.; Havu, P.; Havu, V.; Ren, X.; Reuter, K.; Scheffler, M., Ab initio molecular simulations with numeric atom-centered orbitals. *Computer Physics Communications* **2009**, *180* (11), 2175-2196.

7. Krukau, A. V.; Vydrov, O. A.; Izmaylov, A. F.; Scuseria, G. E., Influence of the exchange screening parameter on the performance of screened hybrid functionals. *The Journal of Chemical Physics* **2006**, *125* (22), 224106.
8. Momma, K.; Izumi, F., VESTA 3 for three-dimensional visualization of crystal, volumetric and morphology data. *Journal of Applied Crystallography* **2011**, *44* (6), 1272-1276.
9. Grimme, S.; Antony, J.; Ehrlich, S.; Krieg, H., A consistent and accurate ab initio parametrization of density functional dispersion correction (DFT-D) for the 94 elements H-Pu. *The Journal of Chemical Physics* **2010**, *132* (15), 154104.
10. Grimme, S.; Ehrlich, S.; Goerigk, L., Effect of the damping function in dispersion corrected density functional theory. *Journal of Computational Chemistry* **2011**, *32* (7), 1456-1465.